Physical Properties and Global Modelling of General Fusion's Magnetized Target Fusion Plasma

generalfusion®

Colin P. McNally, Meritt Reynolds, Sandra Barsky, Samuel Jones, Neeraj Kumar, Zahra Seifollahi Moghadem, Leopoldo Carbajal, Abetharan Antony

General Fusion Inc., Vancouver, British Columbia, Canada

64th Annual Meeting of the APS Division of Plasma Physics, Spokane, Washington, October 17-21, 2022 **UP11.00006**

generalfusion®

Scales and Regimes

General Fusion (GF) is aiming to build fusion power plants using Magnetized Target Fusion (MTF). In a GF-MTF device a three step process occurs: Starting with coaxial helicity injection, plasma is formed into a spherical tokamak. A moving liquid metal wall moves inward and the injector mouth is closed off. Finally the plasma is compressed and reaction rates peak. This novel scheme poses unique problems in realizing the appropriate physics and numerics required to simulate such a system.
In the table below we summarize characteristic, anticipated scales and properties relevant to the design of whole-device modelling codes for a large MCF tokamak (ITER-like) and a GF-MTF power plant device [1]. These dictate the differences between the simulation requirements for the design and characterization of a GF-MTF device and an MCF tokamak.
For both devices we consider a Deuterium plasma. Parameters are from designs where possible, and filled in with projections where needed. Note that for all devices, multiple operational modes are possible with the same hardware. In this table we have attempted to choose values which combine feasability with exploring the envelope of possible configurations a MTF simulation code must handle to be practically useful.

Quantity	Symbol	Formula	MCF Tokamak (∼ITER)	GF-MTF uncompressed	GF-MTF compressed
			Geometry		
Major radius	R_0		6.2 m	1.2 m	0.12 m
Minor radius	a		2 m	0.8 m	0.08 m
Linear Compression Ratio			1	1	10
Volumetric Compression Ratio			1	1	1000
Inverse Aspect Ratio	ϵ	a/R_0	0.32	0.67	0.67
Field Topology			Diverted	Diverted	Wall-limited
			Core Plasma		
Toroidal Field on Magnetic Axis	B_0		5.7 T	0.7 T	70 T
Electron Density (average over core)	n_e		$10^{20}\,\mathrm{m^{-3}}$	$2\times10^{20}\,\mathrm{m^{-3}}$	$4\times10^{23}\,\mathrm{m^{-3}}$
Electron Temperature (average over core)	T_e		13 keV	0.3 keV	12 keV
Ion Temperature (average over core)	T_i		13 keV	0.3 keV	12 keV
Beta Toroidal	β_t	$2\mu_0\langle p_\mathrm{th}\rangle/B_0^2$	3 %	10 %	40 %
Debye Length	λ_D	$\sqrt{\varepsilon_0 k T_\mathrm{e}/n_\mathrm{e} q_\mathrm{e}^2}$	$6.0\times10^{-5}\,\mathrm{m}$	$9.1\times10^{-6}\,\mathrm{m}$	$1.8\times10^{-6}\,\mathrm{m}$
Electron Inertial Length	d_e	$\sqrt{m_\mathrm{e}/n_\mathrm{e} q_\mathrm{e}^2\mu_0}$	$5.3\times10^{-4}\,\mathrm{m}$	$3.8\times10^{-4}\,\mathrm{m}$	$1.2\times10^{-5}\,\mathrm{m}$
Electron Gyrofrequency	Ω_e		$1.0\times10^{12}\,\mathrm{rad\ s^{-1}}$	$1.2\times10^{11}\,\mathrm{rad\ s^{-1}}$	$1.2\times10^{13}\,\mathrm{rad\ s^{-1}}$
Electron Gyroradius	ρ_e	$v_\mathrm{th,e}/\Omega_\mathrm{e}$	$6.7\times10^{-5}\,\mathrm{m}$	$8.3\times10^{-5}\,\mathrm{m}$	$5.3\times10^{-6}\,\mathrm{m}$
Ion Inertial Length	d_i	$\sqrt{m_\mathrm{i}/n_\mathrm{i} q_\mathrm{i}^2\mu_0}$	$5.3\times10^{-4}\,\mathrm{m}$	$3.8\times10^{-4}\,\mathrm{m}$	$1.2\times10^{-5}\,\mathrm{m}$
Ion Gyroradius	ρ_i	$v_\mathrm{th,i}/\Omega_\mathrm{i}$	$4.0\times10^{-3}\,\mathrm{m}$	$5.1\times10^{-3}\,\mathrm{m}$	$3.2\times10^{-4}\,\mathrm{m}$
Ion Plasma Frequency	$\omega_\mathrm{p,i}$	c/d_i	$9.8\times10^{4}\,\mathrm{rad\,s^{-1}}$	$1.4\times10^{5}\,\mathrm{rad\,s^{-1}}$	$4.4\times10^{6}\,\mathrm{rad\,s^{-1}}$
Electron-Electron Collision Time	τ_ee	$1/\nu_\mathrm{ee}$	$2.0\times10^{-4}\,\mathrm{s}$	$5.4\times10^{-7}\,\mathrm{s}$	$1.2\times10^{-7}\,\mathrm{s}$
Total Electron Collision Time	τ_e	$1/(\nu_\mathrm{ee}+\nu_\mathrm{ei})$	$9.0\times10^{-5}\,\mathrm{s}$	$2.5\times10^{-7}\,\mathrm{s}$	$5.5\times10^{-8}\,\mathrm{s}$
Electron Mean Free Path	λ_e		$6\times10^{3}\,\mathrm{m}$	3 m	4 m
Ion Mean Free Path	λ_i		$6\times10^{3}\,\mathrm{m}$	3 m	4 m
Electron-Ion Energy Exchange Time	τ_ex		$6.4\times10^{-1}\,\mathrm{s}$	$1.7\times10^{-3}\,\mathrm{s}$	$3.8\times10^{-4}\,\mathrm{s}$
Electron Hall Parameter		$\Omega_\mathrm{e}/\nu_\mathrm{ei}$	1.7×10^{8}	5.7×10^{4}	1.3×10^{6}
Ion Collisionality / Ion Gyrofrequency	$\nu_{ii}/\Omega_\mathrm{i}$		3×10^{-7}	9×10^{-4}	4×10^{-5}
Ion Gyroradius / Minor Radius	ρ_i/a		2×10^{-3}	6×10^{-3}	4×10^{-3}
Fusion Alpha Gyroradius / Minor Radius	ρ_α/a		2×10^{-2}		5×10^{-2}
			Trapped Particles and Transport		
Banana Orbit Safety Factor	q_b		2	1.5	1.5
Electron Banana Orbit Collisionality	ν_e^*		6×10^{-3}	7×10^{-1}	5×10^{-2}
Ion Banana Orbit Collisionality	ν_i^*		5×10^{-3}	6×10^{-1}	4×10^{-2}
Electron Banana Orbit Width	$\delta_\mathrm{b,e}$	$\rho_\mathrm{e} q_\mathrm{b}/\sqrt{\epsilon}$	$1.5\times10^{-4}\,\mathrm{m}$	$9.3\times10^{-3}\,\mathrm{m}$	$9.7\times10^{-6}\,\mathrm{m}$
Ion Banana Orbit Width	$\delta_\mathrm{b,i}$	$\rho_\mathrm{i} q_\mathrm{b}/\sqrt{\epsilon}$	$1.4\times10^{-2}\,\mathrm{m}$	$9.3\times10^{-3}\,\mathrm{m}$	$5.9\times10^{-4}\,\mathrm{m}$
			Mechanical Equilibrium Timescale		
Alfvén Speed	v_A	$B_0/\sqrt{\mu_0 n_i m_i}$	$8.8\times10^{6}\,\mathrm{m\,s^{-1}}$	$7.7\times10^{5}\,\mathrm{m\,s^{-1}}$	$2.4\times10^{6}\,\mathrm{m\,s^{-1}}$
Lundquist Number	Lu	$a v_\mathrm{A}/\eta_{\perp\mathrm{spitzer}}$	10^{8}	10^{4}	10^{6}
Alfvén Crossing Time		$2\pi R_0/v_\mathrm{A}$	$4.5\times10^{-6}\,\mathrm{s}$	$9.9\times10^{-6}\,\mathrm{s}$	$3.1\times10^{-7}\,\mathrm{s}$
Shot / Compression Timescale			$4\times10^{3}\,\mathrm{s}$	—	$5\times10^{-2}\,\mathrm{s}$
			Scrape off Layer Parallel Heat Transport		
Safety Factor adjacent SOL	q_{95}		4	3	2
SOL Characteristic Length	L_SOL	$2\pi R_0 q_{95}$	160 m	23 m	1.5 m
SOL Electron Temperature	$T_\mathrm{e,SOL}$		190 eV	10 eV	200 eV?
SOL Upstream Electron Density	$n_\mathrm{e,SOL}$		$5\times10^{19}\,\mathrm{m^{-3}}$	$4\times10^{19}\,\mathrm{m^{-3}}$	$1\times10^{23}\,\mathrm{m^{-3}}$
SOL Relative Collisionality	ν^*_SOL	$(L_\mathrm{SOL}/\lambda_\mathrm{e,SOL})/\nu^*_\mathrm{SOL,ITER}$	1	30	13
			Asymmetry		
Field or Wall Toroidal Asymmetry			< 1 %	1 %	1% – 10%?

Here we do not attempt to consider elongation of the plasma. However MTF devices can be designed with significant elongation.

As magnetic flux is lost to the resistive wall the diverted configuration may change. Arrangements with an initially inboard (shaft) limited plasma are also possible.

Temperature increase dominates density increase in compression to raise mean free paths.

Gyrokinetic theory is applicable as in MCF.

Banana orbit dominated due to collisionality in compressed state << 1, Neoclassical contributions important.

Compression time << Alfven crossing time = Plasma close to mechanical equilibrium

The outer flux surfaces (with highest q) will be lost once the plasma becomes wall-limited on the way to peak compression [2,3,4].

Density increases in edge during MTF compression likely making it more collisional, unlike MCF tokamaks which stay semi-collisional.

While for a MCF tokamak the toroidal field asymmetry is largely a matter of well understood design, the ability to capture significant (10%) asymmetry is a design goal for GF-MTF simulation tools.

See also in this session:
UP11.00144 Magnetized Target Fusion Using Mechanically-Driven Liquid Metal Liner **UP11.0007** Steps towards 3D Integrated System Model of Magnetized Target Fusion at General Fusion
UP11.00008 Improved magnetic diagnostics on General Fusion Plasma Injector 3 *Other GF posters:* BP11.00003 CP11.00013 JM09.00015 JP11.00145 PP11.00037 PP11.00090 PP11.00110

References: [1] Laberge 2019, J. Fusion Energy 38:199-303 doi:10.1007/s10894-018-0180-3 [2] Brennan et al. 2021 Nuclear Fusion, 046047 2021 doi:10.1088/1741-4326/abe68c [3] Brennan et al. 2020 Nuclear Fusion, 046027 doi:10.1088/1741-4326/ab74a2 [4] Reynolds 2020 APS Division of Plasma Physics Meeting 2020, abstract id.JO09.006 [5] Zhang et al. 2019, J. Open Source Software 4(37) 1370, doi:10.21105/joss.01370

MTF Whole-Device Modelling

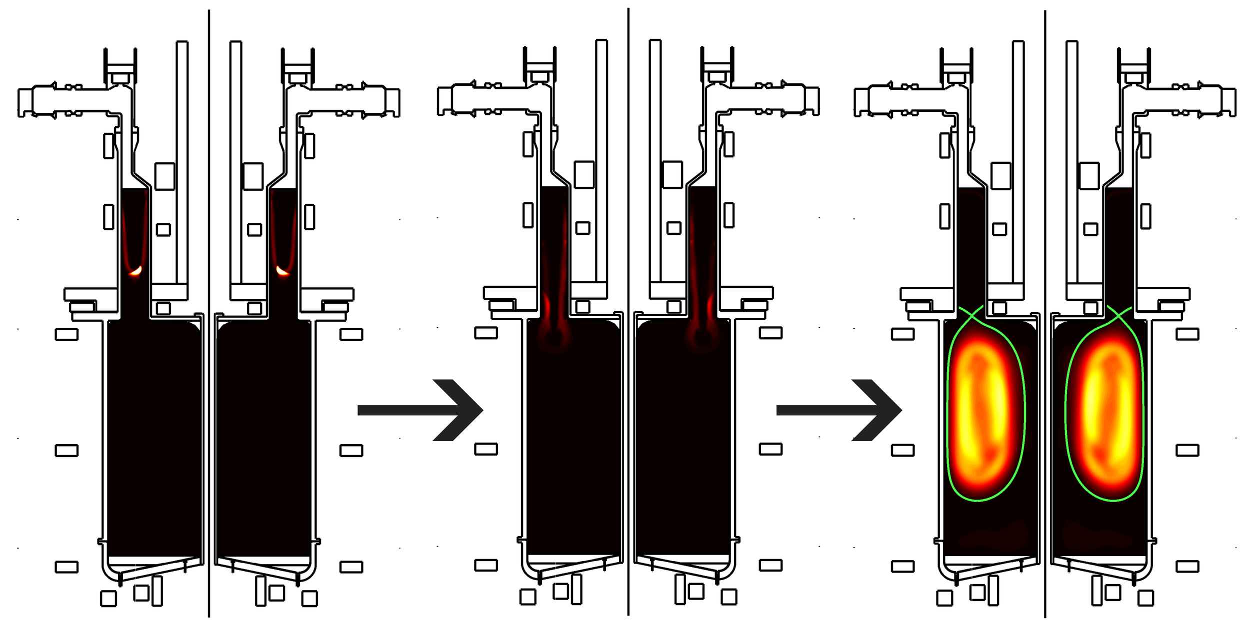

In predicting the fusion yield for a MTF device, the desired capabailites for whole device modelling include
- 3D dynamics of the liquid metal wall
- Wall interaction with the plasma through magnetic fields, forces, and heat loads
- Impurity production, transport, and ionization
- Evolution and nonlinear dynamics of the plasma affecting stability and confinement

Left: In the GF-MTF device the plasma is formed by coaxial helicity injection with a Marshall gun. This can be arranged to result in either a diverted plasma, or an inboard-limited plasma. The formation process is illustrated to the right with contours of the plasma pressure in a simulation carried out as a design exercise for an experimental device. The rightmost panel shows the magnetic separatrix as a green curve. An x-point and divertor legs extending into the mouth of the Marshall gun are formed. During compression the gun mouth is closed as the liquid metal wall moves inwards.

- The plasma is initially held off the outer wall by externally imposed flux (patent applied for). However, due to the finite resistivity of the liquid metal, over time this flux (red curves) is lost to outer wall [4]. At late times (right panel) the plasma is significantly compressed, and can become limited directly on the outer liquid lithium wall.
- Modelling the response of the liquid metal wall to the heat fluxes form the plasma, and the response of the plasma (impurity transport, ionization, temperatures) is a key capability for a next generation MTF simulation code.

Right: After the plasma is formed, it is compressed by the shaped radial collapse of the liquid metal outer wall of the device. Shown are a sequence of magnetic field configurations (closed field lines: blue; open field: red) overlaid on the center shaft (brown) plasma volume (light grey) and the inner part of the liquid metal wall (dark grey).

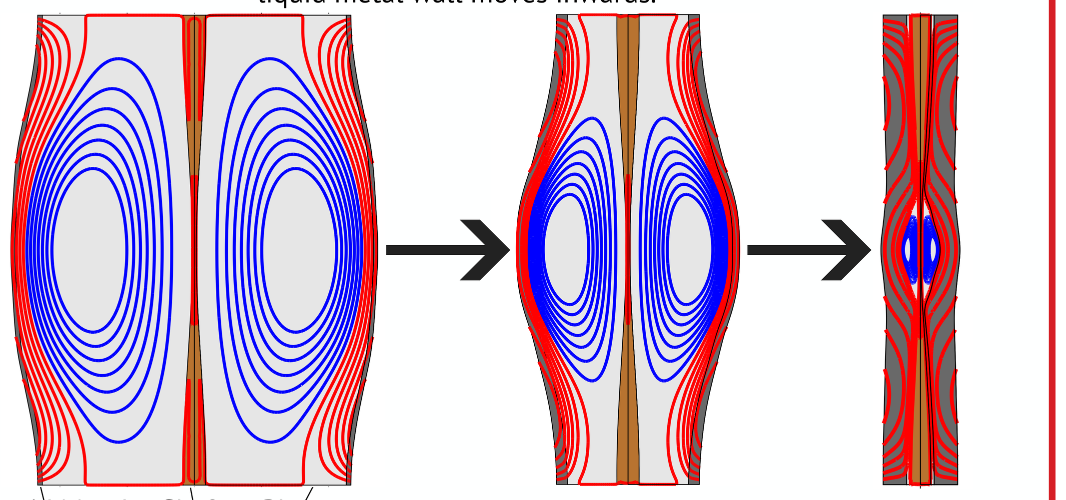

Pulsar: Next Generation Open Source MTF Code Project

To meet the needs of analysis of GF's Fusion Demonstration Plant (FDP) and design of a power plant device, we have begun a project to develop an open-source MTF whole-device modelling code.
- Pulsar must be capable of following the compression to the end of useful fusion yield in three dimensions and capture the mechanical interaction between plasma and liquid metal liner.
- Pulsar must provide results in design-relevant times, so we opt for fluid models with adjustable levels of physics fidelity.
- GF's larger theoretical physics program includes gyrokinetic, edge plasma, plasma-wall interaction, and PIC models of local regions of the plasma.
- Prototyping work has concentrated on employing finite volume (FV) methods and Constrained Transport (CT) on a logically Cartesian Structured Adaptive Mesh Refinement grid.
- Pulsar will use the AMReX block-structured AMR framework (amrex-codes.github.io [5])
- Performance portability across varying CPU and GPU platforms with exascale-capable scaling as design goals.

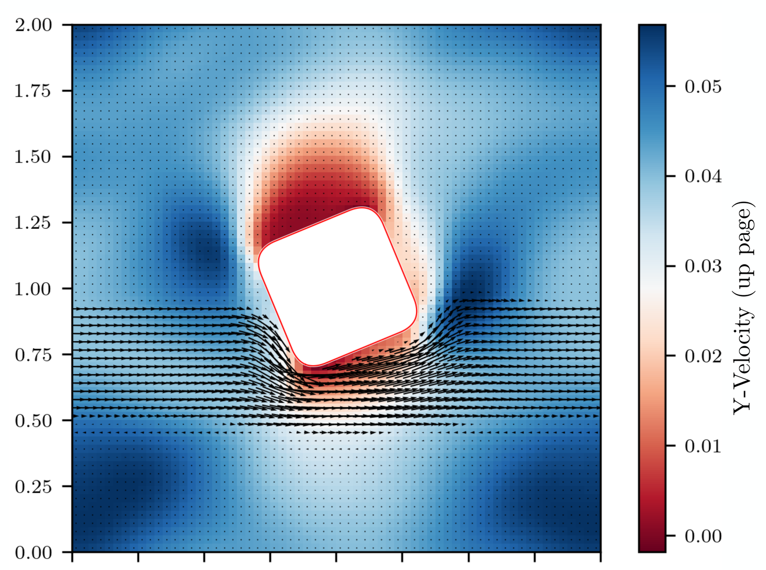

Above: Verification problem of flow of a magnetized plasma flowing around a conducting obstacle. Shown are velocity up the page (colour) and magnetic field (vectors) (Jones et al. in prep).

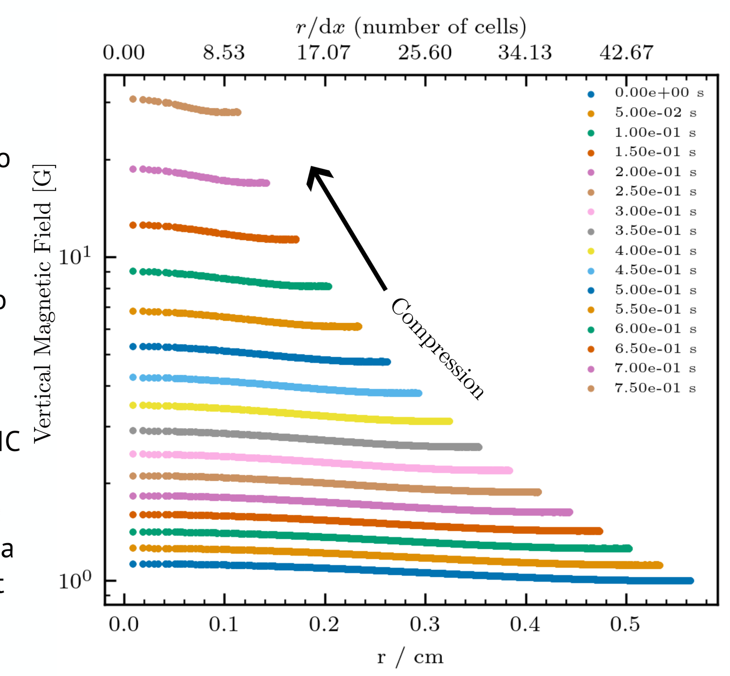

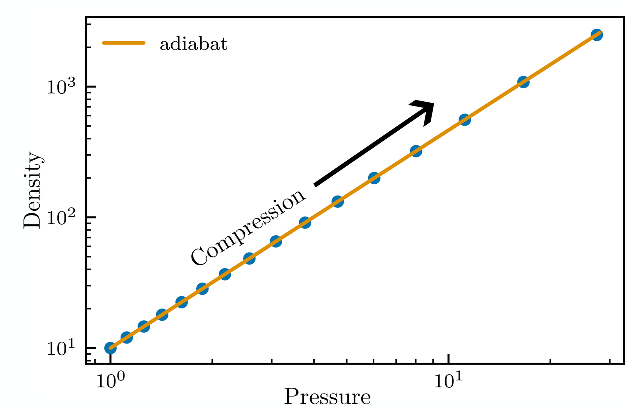

Above: Sub-alfvenic compression of a plasma column.
Top: Vertical component of magnetic field increases as a conducting wall moves radially inwards.
Bottom: Pressure and density increase along an adiabat.

This test demonstrates a novel moving cut-cell embedded boundary implemented in a FV-CT MHD method (Jones et al. in prep). Pulsar will implement a two-sided multifluid version of this to model the compressing liquid metal wall.

Below: Verification of second order accuracy for the diffusion of a magnetic field into a circular plasma in the FV-CT cut-cell method (Jones et al. in prep).

Top: Magnetic field and magnetic pressure at the end state of the problem.
Bottom: L1 norm error converges to the analytical solution at greater than second order.